Received: 21 August 2023 | Revised: 18 October 2023 | Accepted: 26 October 2023

DOI: 10.1002/jcu.23604

RESEARCH ARTICLE

WILEY

Anatomical structure characterization of fetal ultrasound images using texture-based segmentation technique via an interactive MATLAB application

Saulo Molina-Giraldo MD, MSc, PhD (e)[1,2,3] | Natalia Torres-Valencia MD[1,2] | Cristian Torres-Valencia PhD[4] | Hector Fabio Restrepo Msc, PhD (e)[5]

[1]Section of Fetal Therapy and Fetal Surgery Unit, Division of Maternal Fetal Medicine, Department of Obstetrics and Gynecology Hospital de San José, Department of Obstetrics and Gynecology, Fundación Universitaria de Ciencias de la Salud – FUCS, Bogotá, Colombia

[2]Fetal therapy and Surgery Network – FetoNetwork, Bogotá, Colombia

[3]Division of Maternal Fetal Medicine, Department of Gynecology and Obstetrics Faculty of Medicine, Universidad Nacional de Colombia, Bogotá, Colombia

[4]Department of Electronic Engineering, Universidad del Quindío, Armenia, Colombia

[5]Research Division, Fundación Universitaria de Ciencias de la Salud – FUCS, Bogotá, Colombia

Correspondence
Saulo Molina-Giraldo, Maternal Fetal Medicine Unit, Therapy, Fetoscopic and Fetal Surgery Center, Carrera 19C #90-30, 4th floor, Clínica de la Mujer-Grupo Quironsalud, Bogotá, Colombia.
Email: saulo.molina@urosario.edu.co, smolina@fucsalud.edu.co

Abstract

Objective: To describe the texture characteristics in several anatomical structures within fetal ultrasound images by applying an image segmentation technique through an application developed in MATLAB mathematical processing software.

Methods: Prospective descriptive observational study with an analytical component. 2D fetal ultrasound images were acquired in patients admitted to the Maternal Fetal Medicine Unit of the Hospital de San José, Bogotá-Colombia. These images were loaded into the developed application to carry out the segmentation and characterization stages by means of 23 numerical texture descriptors. The data were analyzed with central tendency measures and through an embedding process and Euclidean distance.

Results: Forty ultrasound images were included, characterizing 54 structures of the fetal placenta, skull, thorax, and abdomen. By embedding the descriptors, the differentiation of biologically known structures as distinct was achieved, as well as the non-differentiation of similar structures, evidenced using 2D and 3D graphs and numerical data with statistical significance.

Conclusion: The texture characterization of the labeled structures in fetal ultrasound images through the numerical descriptors allows the accurate discrimination of these structures.

KEYWORDS
diagnostic imaging, image segmentation, MATLAB, prenatal diagnosis, prenatal ultrasonography

1 | INTRODUCTION

An ultrasound image, in its most straightforward concept, is a two-dimensional array of elements, where each one contains a value related to the color or intensity level in the captured scene.[1] In technical terms, this grid is a matrix, and each grid point is a pixel. The dimensions of this matrix directly represent the resolution of the image, that is, the greater the number of pixels, the greater the resolution in the image.[2] The intensity values of the pixels are essential information that forms the image and corresponds to its spatial domain. Many image processing operations are defined in this domain, in pre-processing stages, such as denoising, histogram transformations, and spatial filtering, among others.[3] However, spatial domain processing can also be applied to characterization, segmentation and description of regions stages based on the relationship between the intensities of adjacent pixels and their relative variation, which can be directly related to the textures observed within the image.[4] In this case, the spatial domain processing is applied to improve the interpretability of the information contained in the scene, which may not be apparent enough to the naked eye, taking into account the

different scenarios related to the acquisition technology or ilumination issues. This applies to a greater extent to ultrasound images, which are easily affected by noise due to their capture technology based on ultrasound frequency signals, in addition to the fact that their quality is operator dependent.[5]

Image segmentation is a stage included in image processing systems that allows to partition a scene between the objects that compose it. In medical imaging, segmentation makes it possible to distinguish regions associated with different anatomical structures for more detailed analysis.[6] The distinction of these regions is made by using the information of the pixels through the analysis of high-frequency components such as edges and lines, or by low-frequency components such as the textures of the regions.[7] In medical research, the main objective of segmentation is the separation of different anatomical structures through the extraction and classification of their characteristics.[8] Various data processing platforms could be considered for working with images, acknowledging their matrix structure, and various programming languages that allow building algorithms to solve problems involving images.[9]

In fetal ultrasound images, advances in capture technology and in the medical interpretation of captures have opened the door to the detection of numerous fetal and ovular abnormalities. However, some patterns and data relationships at the pixel level remain difficult to discover despite a high degree of experience in obstetric practice. Therefore, certain image characteristics can be analyzed from the application of computational processing techniques that allow expanding the information obtained, precisely its texture, and in this context, to make precision diagnoses in pregnancy care or even in the planning of fetal surgeries.[10]

Since it is a broad field to be explored that could significantly help prenatal diagnosis in fetal medicine units, this research proposes the characterization of texture in fetal ultrasound images by applying a spatial domain segmentation technique through an application developed in the mathematical processing software MATLAB.

2 | MATERIALS AND METHODS

This is a prospective descriptive observational study with an analytical component. Forty fetal ultrasound images of women with low obstetric risk pregnancies without associated comorbidities and fetuses without known structural or infectious pathology obtained during the second trimester of pregnancy were included. We excluded fetal ultrasound images of women who presented technical difficulties for image acquisition and could not meet acquisition standards due to fetal conditions (fetal position with dorsum anterior or posterior, oligohydramnios or polyhydramnios) or maternal conditions (increased body mass index or maternal abdominal scars).

The development of the project was carried out following a methodology divided into phases:

- *Image selection*: The images were selected from pregnant women who attend ultrasound evaluation (outpatient or emergency) in the Maternal Fetal Medicine Unit of the Hospital de San José Bogotá. These images were obtained with a SAMSUNG Accuvix V10 (Seoul-Korea) ultrasound machine in the "General Obstetrics" preset, with a 10 frames per second and 98 dB acoustic power, using a convex probe working at 3.5 to 5 MHz. Images were taken in classic standardized planes for biometry, as follows: ten axial section images of the fetal brain in the transthalamic plane, ten images of the fetal thorax in a four-chamber view, ten axial section images of the fetal abdomen and ten images longitudinal section of the placenta. Following these stablished settings and the aforementioned acquisition protocol, our aim was to obtain the less variability within the planes and maintain an optimal resolution for the subsequent analysis. These images were downloaded to a *Universal Serial Bus (USB)* 32 Gb device in a *.bmp (bit maps protocol*) format since it is a lossless format, which does not allow altering the information of the pixels when storing it. Subsequently, the images are uploaded to a cloud server from where they are made available for processing on a computer with permission to use the application.
- *Images loading to the application created in MATLAB*: The application was developed using the MATLAB® (*MATrix LABoratory)* mathematical software version 2021a. For a better usability, a user interface was also developed, for the specialist to perform the different stages of image processing, with a module for loading images. Initially, within the applicative, the selected images are loaded and the module is in charge of loading, and showing the image in the interface window.
- *Definition of gray level and threshold parameters*: The processing is performed in the spatial domain of the image by analyzing intensity levels. Within the applicative, the module in charge of this stage allows defining the initial intensity level parameters s and a comparison threshold T, through sliders that will enable interactive modification of their values. The degree of intensity for the present work is defined as the intensity of the pixels, which for the analysis of the ultrasound image, would be represented by the power of the echoes translated in the ultrasound system. The threshold is the minimum or initial point to start the image analysis process. Let $f(x,y)$ be an image function at positions $x,y \in N$, where each position corresponds to a certain intensity level $\rho \in [0,255]$. These intensity levels will be subsequently evaluated together with the s, T parameters to generate the segmented image, understanding segmentation of the image as its partition until a region of interest is achieved with an area defined at the threshold and similar intensity, which allows analysis of the pixel characteristics.
- *Region growing*: It refers to the image region where the pixel analysis began in terms of intensity and threshold. Based on the previously defined parameters, the loaded image is processed and the regions containing pixels that meet the values represented by the two parameters are found. For this, the application uses this region growing strategy which proposes an algorithm as follows[11]:

a. An image $S(x,y)$ is obtained which contains all the "seed" pixels that meet the condition $f(x,y) = s$.

b. The threshold condition is evaluated on each pixel of the image and a certain value is assigned depending on the result: $f_Q(x,y) = \begin{cases} 1 \rightarrow |s - f(x,y)| \leq T \\ 0 \rightarrow |s - f(x,y)| > T \end{cases}$
c. A new image is generated $g(x,y)$ in which only the pixels of $f_Q(x,y)$ are considered which are found 8-connected in the vicinity of each seed $S(x,y)$.
d. Each connected component of $g(x,y)$ is assigned a different label. The software assigns a colorimetric code to differentiate internal or external connected pixels according to intensity and threshold analysis. The color is randomly assigned and does not correlate to the intensity of the analyzed growth area. The latter is assigned by the software according to the specific area of interest given by the user of the image analyzer Figure 1.

- *Regions visualization*: To analyze the segmented regions, the image $g(x,y)$ is presented within the application, containing from 1 to n regions. The labels are associated with each region, as explained above, with a particular color assigned by the function "label2rgb". The regions with their respective colors are presented as an additional image Figure 1.

Different regions will be obtained depending on the parameter values in the segmentation stage. The Maternal Fetal Medicine specialist configures the appropriate values to receive the following structures: in skull images, segmentation and labeling of the proximal calotte, distal calotte, interthalamic midline, anterior midline, median wall of proximal and distal anterior horn, lateral wall of proximal and distal anterior horn, insula, choroid plexus, proximal

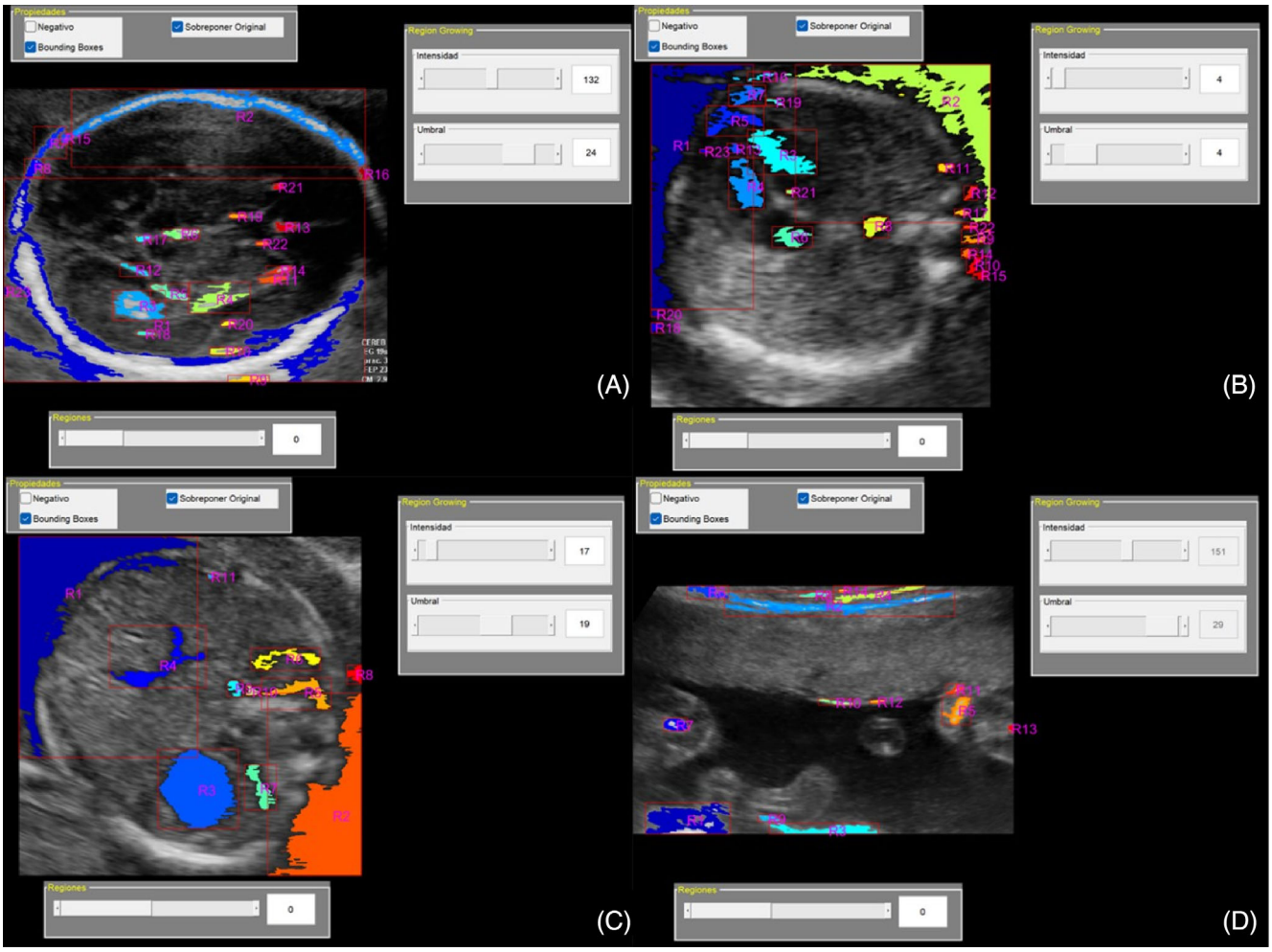

FIGURE 1 Application interface during the segmentation process of loaded images, by means of the growing region technique, where an intensity value and T threshold are defined, from which at least two types of regions are distinguished: those that meet or not, on condition f_Q. In *a*, an image of the fetal skull in transthalamic section is observed, in which with an intensity of 132 and a threshold of 24 it is possible to segment into R2 proximal calotte, R3 choroid plexus, R6 interthalamic midline, R12 parahippocampal gyrus, R13 anterior midline, R14 lateral wall of the distal anterior horn and R21 proximal, R19 medial wall of the proximal anterior horn and R22 distal, R20 insula. In *b*, an image of the fetal thorax in a 4-chamber section is observed, with an intensity of 4 and a threshold of 4, the segmentation of R3 left ventricle, R4 right ventricle, R6 right atrium and R8 descending aorta is performed; *c* shows an image of the fetal abdomen in axial section for biometry, with an intensity of 17 and a threshold of 19, showing the segmentation of R3 gastric chamber, R4 intraabominal umbilical vein, R6 right adrenal gland, and R7 left adrenal gland. Finally, in *d* a longitudinal section of the placenta is observed with an intensity of 151 and a threshold of 29 that shows the segmentation of R2 maternal plate and R10 fetal plate.

thalamus, distal thalamus, proximal peduncle, distal peduncle, parahippocampal gyrus, frontal, parietal, and occipital lobes. In the thorax, we proceed to segment the proximal rib, distal rib, column, skin, right ventricle wall, left ventricle wall, papillary muscle, interatrial septum, interventricular septum, mitral valve, tricuspid valve, right atrium, left atrium, right ventricle, left ventricle, descending aorta, upper and lower left lung, and upper and lower right lung. On the other hand, the abdomen, proximal rib, distal rib, column, skin, gastric wall, gastric chamber, left adrenal gland, right adrenal gland, umbilical vein and liver were obtained. Finally, in the images of the placenta, labeling of amniotic fluid, placenta in the medial region, placenta in the lateral region, fetal plaque, maternal plaque and retroplacental space is performed. Figure 1

- *Region selection*: From each labeled region presented in the image, a selection is made to apply the defined descriptors that allow quantifying the information contained in them.
- *Calculation of descriptors*: Shape and texture descriptors are computed: Solidity, perimeter, average gray level, contrast, smoothness of the image (smoothness), third moment, uniformity, area, centroid x, centroid y, eccentricity, number Euler, entropy, Hu invariant moments (from 1 to 8), gray level and threshold. This stage results in a vector with 23 features (dimensions of each structure), for each segmented and selected structure M_i.
- *Data export*: The data generated by the application is derived in terms of quantitative variables to a *.csv* format, which is exported to an Excel database and subsequent transformation to a MATLAB statistical package for analysis.
- *Data analysis*: The characteristics of each image were analyzed in terms of their statistical moments with measures of central tendency: mean and standard deviation. Due to the size of the chosen sample, represented in the number of images used that in turn are translated into different segmented regions, the amount of data obtained is considerably high in computational terms. In addition, each data is represented in 23 dimensions associated with the descriptors, which made it necessary to use a representation technique that facilitates its analysis and comparison between segmented structures across all the images. This is why an embedding process is performed in order to bring the 23 descriptors obtained for each image (23 dimensions) to 2 or 3 dimensions (as configured within the algorithm). This procedure uses the *t-distributed Stochastic Neighbor Embedding (tSNE)* method. This method assumes Gaussian distribution functions on each data (M_i structure) in the original dimension (23D), and the probability that the other data M_j belong to said distribution is calculated[12]:

$$p_{ij} = \frac{exp(-||M_i - M_j||2/2\sigma 2)}{\sum_{k \neq l} exp(-||M_k - M_l||2/2\sigma 2)}$$

Then we proceed to create a smaller dimensional space with the coordinates of the structures in a random way using a t-student distribution in 2 or 3 dimensions. These random coordinates are fitted by the Kullback Leibler (KL) distance, minimizing the distances between the distributions in normal space and embedded space. The coordinates are taken to the domain from −1 to 1 by a scale normalization and, since it is a stochastic process, it is repeated 10 times each for the statistical validity of the results. Finally, to determine the set of morphological and statistical measurements that allow optimally differentiating the anatomical regions evaluated, the Euclidean distance is applied $D(M_i, M_j) = \sqrt{\sum_{k=1}^{n} (M_{i,k} - M_{j,k})2}$ with k representing each dimension of embedment from 1 to 2 or 3 depending on the selection, between each pair of structures in the lower dimension space. Statistical moments such as the mean and variance of said distances are obtained from this analysis, necessary to determine the most discriminating characteristics from the greatest distances obtained.

The Pearson correlation coefficient was applied to these data, taking as H0 the similarity of the structures and H1 the difference between them, considering $p < 0.05$ as significant.

To control selection bias, the selected images must comply the standardized parameters for taking fetal biometrics from international (ISUOG)[13] and national (FECOPEN) guidelines.[14] In order to avoid the loss of information contained in the image, the use of the image format that loses less information is considered, which is *.bmp*, since in this the pixel information is stored through a bit level without any compression. Additionally, in the image loading process, MATLAB asigns two-dimensional array according to the bitmap file, with which the information of each pixel is exactly that stored in the file. When working with an embedding process based on probability distribution functions, there is a certain degree of randomness in the procedure, therefore, the same procedure was carried out 10 times to ensure its statistical validity. Despite all the uniform technical and protocol conditions that are used to start the segmentation process in the application, the definition of intensity and threshold levels, as well as the labeling of the regions is a task performed by a human operator.

Ethical considerations: This research protocol was presented to the institutional ethics committee where it was considered a risk-free research.

3 | RESULTS

In total, forty fetal ultrasound images that met the indicated inclusion and exclusion criteria were included. The mean gestational age of the pregnancies included was 21.5 +/− 2.2 (19.3–23.7) weeks. After analyzing the data obtained from the 23 descriptors for each of the structures of the different images, the following characteristics were obtained: for each skull image, 18 structures were considered, obtaining a total of 414 texture descriptor data, with a total of 4140 data for all fetal skull images. In each of the thorax images, 20 structures were labeled, which generated 460 descriptor data, for a total of 4600 for all fetal thorax images. Likewise, for the images of the fetal abdomen, ten structures were used, obtaining 230 descriptor data per image and a total of 2300 for the set of abdomen images. Finally, 6 structures were labeled for the placenta images, receiving 138 descriptor numerical data for each image and a total of 1380 data for all the placenta images. In the end, raw data of the 23 descriptors were obtained for

each of the 54 labeled structures, with a total of 12 420 pieces of data, which were normalized by z-score and grouped in means and variances to analyze the distance to the centroid of the model. Subsequently, to achieve the analysis and representation of the data, the 23 dimensions associated with the descriptors were taken to the embedding process in order to be reduced to 2 and 3 dimensions. The embedding of the data was carried out in 10 repetitions, then means and variances were obtained for each of them, which were plotted in 2D and 3D planes compared to other structures (comparison in graphs 1 to 1 and in the same graph with all the other structures of the section) which allows observing the discrimination that embedment makes in the search of structures that are biologically and histologically different, as well as keeping a similar dispersion of the data in those structures that are presumed to have a similar macroscopic and microscopic texture (same structure on the other side of the midline, same structure in another case or structure with similar histology). In Figures 2–5 it is possible to observe the 2D and 3D graphic distribution of the data derived from the embedding process for representative structures of the skull, thorax, abdomen and placenta respectively, showing the distribution of the means of each case at its centroid, and the relationship of the data of each structure with others, whether they are of biology known to be similar or not. When the descriptors were analyzed individually, it was striking that, in the cerebral lobes, the Hu moments were the descriptors that consistently had a high correlation with significant p values ($p = 0.000$).

The Euclidean distance was applied to each of the cases in all the structures and their centroid, again obtaining means and variances, with which a lower value is observed numerically between data belonging to the same anatomical structure (intra-structure), and greater distances in structures in which a biologically different texture is known (between structure). In Tables 1–4, distance is classified into three categories, green for distances less than 0.5, yellow for distances between 0.51 and 0.80, and orange for distances greater than 0.81. In all these tables, the intra-structure distances are consistently observed on the diagonal, which works as a control, these being the shortest distances found. Marked as green, but with a slightly greater distance than the previous ones, are the homologous structures on the other side of the midline, such as the proximal and distal calotte (Table 1), the proximal and distal rib (Table 2), and the right adrenal and left (Table 3). The other short distances found are when comparing structures with known biological similarity, thus in Table 1, those structures of interfaces and convolutions (anterior and interthalamic midline, medial and lateral wall of anterior and posterior horns, insula and parahippocampal gyrus), thalami and peduncles and grouping of cerebral lobes. In Table 2, the grouping of structures formed by myocardium (right ventricle wall, left ventricle wall, papillary muscle, interatrial septum, interventricular septum, mitral valve, tricuspid valve), among these also being the shortest distances between the structures of greater similarity such as tricuspid valve versus mitral valve, and interatrial septum versus interventricular septum; in addition to middle versus lateral placenta and maternal plaque versus fetal

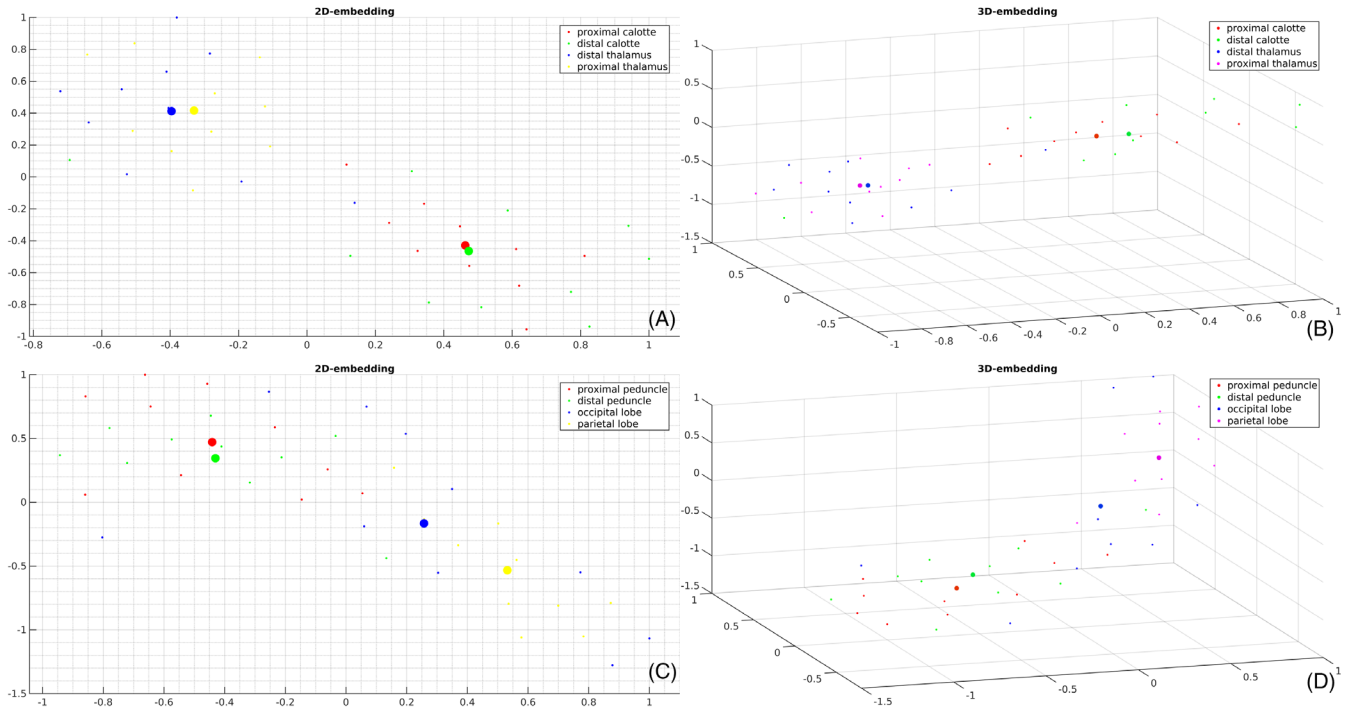

FIGURE 2 2D and 3D graphs that represent the process of embedding texture descriptors in fetal skull structures, showing the centroid of each structure in the larger colored circles and each point associated with the structure in smaller size. M_i. In *a* and *b* the distribution of embedded data is observed for the proximal thalamus, distal thalamus, proximal calotte and distal calotte, observing a similar dispersion of the data for the first two and also for the last two, but keeping a clear distribution difference between these pair of structures. In *c* and *d*, the data of the distal peduncle, proximal peduncle, occipital lobe and parietal lobe are observed, again showing a similar distribution of the means of the first two structures and their differentiation with the last two, which in turn have a related spatial distribution.

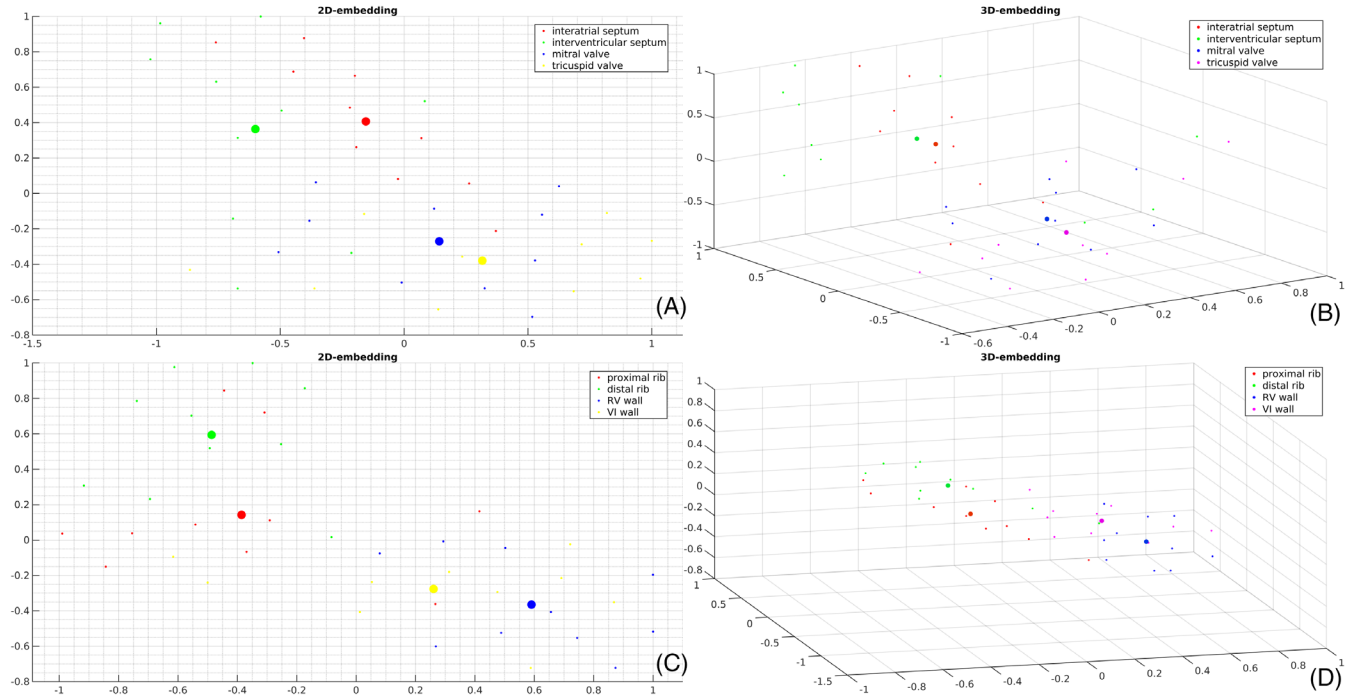

FIGURE 3 2D and 3D graphs that represent the process of embedding texture descriptors in fetal thorax structures, showing the centroid in the larger colored circles and the smaller each point associated with the structure M_i. In *a* and *b* the distribution of embedded data of the interatrial septum, interventricular septum, mitral valve and tricuspid valve is observed; showing a similar distribution of the data for the first two structures and for the last two. In *c* and *d* the data of proximal rib, distal rib, RV wall (Right ventricle wall) and VI wall (left ventricle wall) are plotted, again similar distributions are observed for biologically similar structures.

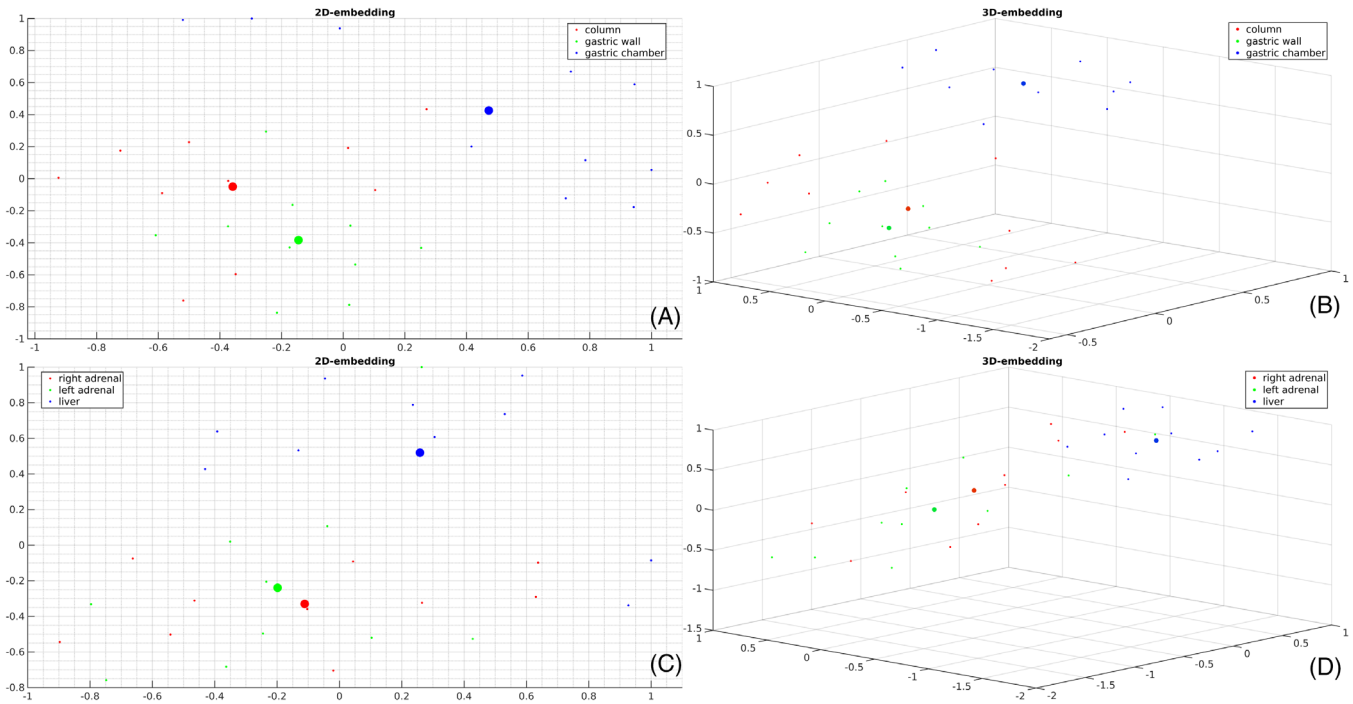

FIGURE 4 2D and 3D graphs that represent the process of embedding texture descriptors in fetal abdomen structures, showing the centroid in the larger colored circles and the smaller each point associated with the structure M_i. In *a* and *b*, the embedded data of the right adrenal, left adrenal, and liver are plotted, showing a clear trend towards a similar distribution for the first two, and an evident difference with the data of the liver structure. In *c* and *d* the data distribution of the column, gastric wall and gastric chamber are observed, observing a separation of the data of the last structure that, unlike the first two, has an aqueous content.

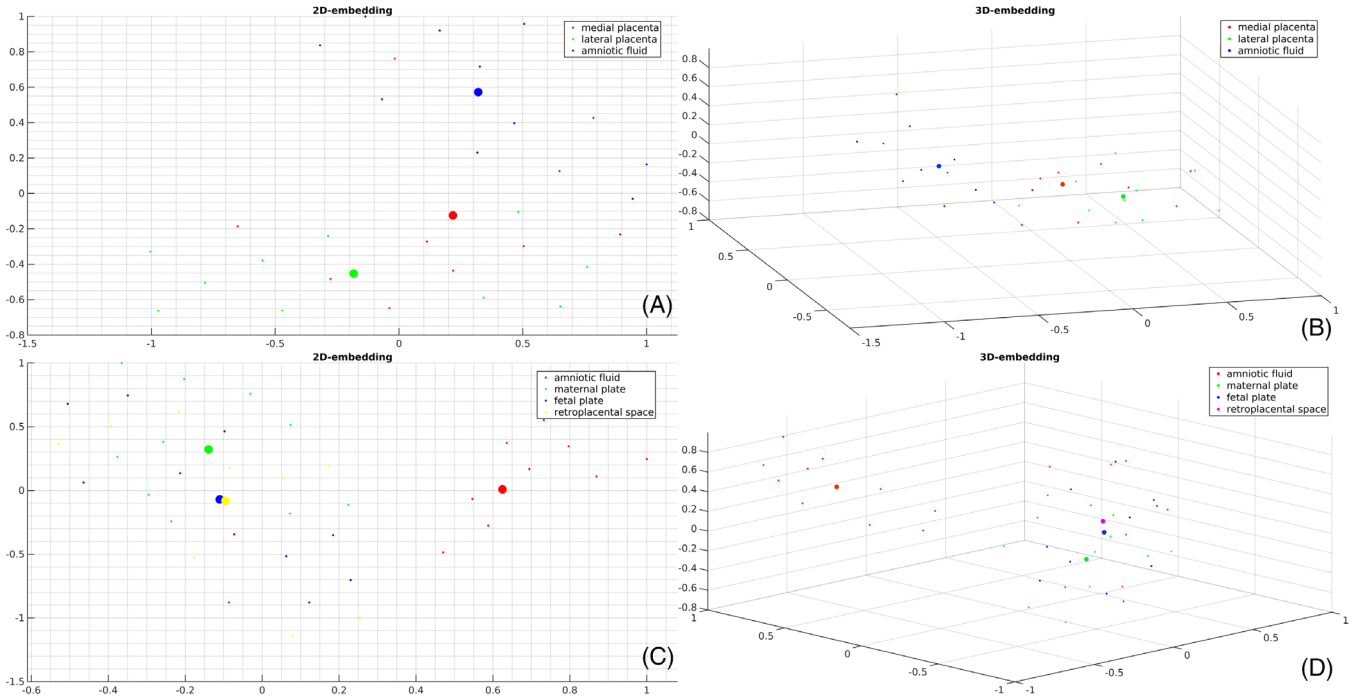

FIGURE 5 2D and 3D graphs that represent the process of embedding texture descriptors in placenta structures, showing the centroid in the larger colored circles and the smaller each point associated with the structure M_i. In *a* and *b*, the distribution of means of medial placenta, lateral placenta and amniotic fluid is observed, observing a separation of the data of the last structure which, unlike the first two, is aqueous. In *c* and *d* the data of amniotic fluid, maternal plate and retroplacental space are observed, again observing a clear separation of the first structure from the others, due to its nature of liquid.

plaque in Table 4. Intermediate distances, marked in yellow, were also obtained from structures whose content is similar, such as those that contain liquid, and is the case of the umbilical vein versus gastric chamber in Table 3. The greatest distances obtained, marked in orange, were those found between structures of different known histology such as skull versus interface structures and gyri in Table 1; in Table 2, ribs versus myocardial-derived structures, blood-containing structures (right atrium, left atrium, left ventricle, and right ventricle) versus myocardial-derived structures, and lungs versus myocardial-derived structures; in Table 3 the grouping of osteocartilaginous structures (proximal rib, distal rib and column), skin and muscles (gastric wall) versus structures containing fluid (umbilical vein and gastric chamber), and amniotic fluid versus placental tissue in Table 4.

Finally, comparing the Euclidean distances between structures yielded significant p (<0.05) in multiple descriptors between structures of different presumed textures, evidencing the differentiation of structures by texture descriptors. As well as finding a non-significant difference in the distance of structures known to be similar: proximal thalamus versus distal thalamus ($p = 0.827$), mitral valve versus tricuspid valve ($p = 0.704$), left adrenal versus right adrenal ($p = 0.489$), and fetal plaque versus maternal placental plaque ($p = 0.407$). Table 5.

4 | DISCUSSION

The use of image segmentation is motivated by the possibility of divide or separate the image into regions with similar attributes, being one of the first steps in analysis and scene interpretation.[5] In general, image processing applications are focused on intensity or grayscale analysis,[15] and specifically, image segmentation in medical research seeks to separate and differentiate anatomical structures through the extraction and classification of features.[8] However, these could also lead to a processing system that aims to improve the interpretability of the information contained in the pixels, such as texture. Moreover, to efficiently reflect these advantages of image processing to clinical process, the features extracted and the segmented regions could be presented to ultrasound specialists that are interested on fetal diagnosis. The use of user interface that interactively perform segmentation of anatomical structures in fetal ultrasonography will facilitate visualization and understanding of the present information.

Our results achieved the characterization of the texture of fetal placenta, skull, thorax, and abdomen structures (54 structures in total) in ultrasound images by means of 23 numerical descriptors. It is noteworthy that when loading the images of any of the four slices into the application, after the segmentation and labeling of the structures, it is able to recognize similar and opposite texture features, that is, echographically similar attributes (hyper, hypo, or anechoic) are recognized by the derived methodology. This is demonstrated because when comparing the differentiation capacity of the application, after the segmentation of the 18 labeled structures in fetal skull images, and application of the embedding process and Euclidean distance, there were statistically significant graphic and numerical differences between structures with biological known as distinct ($p < 0.000$). When segmenting areas such as thalami on each side of the midline,

TABLE 1 Mean embedment distances within structures and between structures in the image of the fetal skull in transthalamic section.

Structure	ITM	PAHM	DAHM	AML	Insula	CP	PC	DC	DT	DP	PP	PT	PAHL	DAHL	OL	PL	FL	PHG
ITM	0,368	0,351	0,393	0,368	0,384	0,874	1561	1477	0,519	0,384	0,395	0,528	0,524	0,434	0,720	1102	0,946	0,364
PAHM	0,394	0,357	0,363	0,388	0,398	1066	1747	1663	0,598	0,382	0,411	0,617	0,429	0,379	0,892	1293	1139	0,368
DAHM	0,422	0,334	0,309	0,407	0,421	1184	1867	1783	0,683	0,375	0,434	0,707	0,338	0,311	1007	1412	1257	0,359
AML	0,489	0,486	0,508	0,487	0,495	0,925	1594	1511	0,616	0,491	0,498	0,627	0,587	0,528	0,798	1143	0,992	0,484
Insula	0,410	0,423	0,468	0,404	0,394	0,891	1571	1487	0,486	0,409	0,405	0,502	0,576	0,499	0,720	1119	0,966	0,409
CP	0,900	1049	1169	0,911	0,886	0,409	0,699	0,624	0,636	0,972	0,883	0,618	1340	1227	0,432	0,433	0,414	0,987
PC	1559	1730	1854	1577	1554	0,695	0,141	0,163	1233	1654	1548	1207	2028	1913	0,880	0,467	0,624	1668
DC	1563	1702	1809	1576	1554	0,859	0,367	0,403	1295	1635	1551	1274	1964	1860	1009	0,677	0,803	1648
DT	0,469	0,588	0,688	0,474	0,477	0,684	1237	1155	0,419	0,541	0,453	0,429	0,838	0,736	0,570	0,837	0,723	0,540
DP	0,502	0,488	0,501	0,493	0,491	0,984	1668	1584	0,561	0,478	0,491	0,572	0,545	0,508	0,809	1213	1058	0,484
PP	0,416	0,441	0,497	0,409	0,412	0,880	1560	1477	0,476	0,412	0,399	0,489	0,594	0,525	0,729	1105	0,950	0,418
PT	0,448	0,578	0,681	0,459	0,457	0,551	1209	1128	0,332	0,529	0,437	0,331	0,844	0,731	0,449	0,752	0,602	0,530
PAHL	0,564	0,436	0,371	0,546	0,565	1367	2048	1965	0,862	0,491	0,574	0,885	0,325	0,349	1191	1595	1440	0,478
DAHL	0,510	0,425	0,389	0,500	0,515	1262	1939	1855	0,768	0,466	0,526	0,789	0,384	0,379	1086	1487	1334	0,453
OL	0,881	1004	1097	0,896	0,884	0,595	0,908	0,853	0,705	0,955	0,879	0,690	1239	1143	0,592	0,666	0,613	0,961
PL	1101	1271	1395	1118	1096	0,318	0,466	0,385	0,772	1195	1088	0,747	1569	1453	0,456	0,236	0,272	1208
FL	0,990	1139	1257	1001	0,983	0,545	0,654	0,599	0,759	1069	0,971	0,747	1426	1314	0,605	0,495	0,526	1080
PHG	0,412	0,394	0,416	0,403	0,403	0,998	1681	1597	0,543	0,394	0,408	0,559	0,487	0,434	0,821	1226	1071	0,390

Note: The distance is classified into three categories, green for distances less than 0.5, yellow for distances between 0.51 and 0.80, and orange for distances greater than 0.81.
Abbreviations: AML, anterior midline; CP, choroid plexus; DAHL, distal anterior horn lateral wall; DAHM, distal anterior horn medial wall; DC, distal calotte; DP, distal peduncl; DT, distal thalamus; FL, frontal lobe; ITM, interthalamic midline; OL, occipital lobe; PAHL, proximal anterior horn lateral wall; PAHM, proximal anterior horn medial wall; PC, proximal calottee; PHG, parahippocampal gyrus; PL, parietal lobe; PP, proximal peduncle; PT, proximal thalamus.

TABLE 2 Mean embedment distances within structures and between structures in the four-chamber section of the fetal thorax image.

Structure	PR	Skin	DR	Column	RVW	LVW	PM	IAS	IVS	MV	TV	DAo	RA	LA	LV	RV	ULL	LLL	URL	LRL
PR	0,418	0,463	0,703	0,937	1175	0,802	1359	1014	0,897	1396	1451	1076	0,679	0,518	0,443	0,547	0,583	0,553	0,666	0,674
Skin	0,555	0,501	0,848	0,798	1014	0,692	1186	0,865	0,770	1227	1282	0,932	0,812	0,505	0,531	0,518	0,703	0,531	0,810	0,819
DR	0,695	0,840	0,340	1520	1782	1367	1966	1614	1490	2007	2062	1686	0,365	0,920	0,755	0,965	0,639	0,959	0,463	0,453
Column	0,944	0,773	1541	0,462	0,545	0,485	0,623	0,481	0,485	0,673	0,713	0,544	1502	0,700	0,873	0,663	1159	0,683	1419	1435
RVW	1190	1008	1795	0,501	0,406	0,571	0,422	0,447	0,499	0,439	0,461	0,446	1750	0,916	1113	0,869	1410	0,898	1677	1693
LVW	0,784	0,666	1371	0,441	0,534	0,402	0,665	0,456	0,422	0,706	0,755	0,499	1329	0,608	0,732	0,582	0,995	0,593	1249	1265
PM	1369	1185	1976	0,540	0,354	0,655	0,297	0,459	0,550	0,312	0,319	0,436	1932	1091	1291	1042	1582	1067	1855	1870
IAS	1002	0,819	1616	0,320	0,321	0,380	0,398	0,299	0,332	0,439	0,489	0,345	1574	0,730	0,927	0,684	1224	0,711	1493	1509
IVS	0,893	0,712	1501	0,457	0,490	0,455	0,593	0,450	0,441	0,611	0,652	0,473	1456	0,631	0,818	0,597	1124	0,630	1384	1400
MV	1395	1209	2008	0,541	0,265	0,661	0,174	0,431	0,534	0,149	0,153	0,353	1961	1114	1317	1063	1614	1088	1888	1904
TV	1462	1278	2071	0,625	0,368	0,743	0,252	0,521	0,619	0,229	0,217	0,443	2024	1184	1385	1134	1680	1159	1953	1969
DAo	1084	0,901	1692	0,453	0,364	0,491	0,423	0,402	0,423	0,432	0,467	0,356	1645	0,811	1007	0,761	1311	0,791	1576	1592
RA	0,585	0,766	0,172	1480	1736	1323	1921	1572	1444	1960	2015	1637	0,139	0,860	0,661	0,908	0,536	0,905	0,340	0,333
LA	0,568	0,515	0,946	0,691	0,888	0,608	1071	0,732	0,659	1112	1168	0,811	0,910	0,498	0,539	0,496	0,724	0,506	0,879	0,889
LV	0,514	0,513	0,720	0,854	1100	0,727	1279	0,937	0,832	1322	1377	1017	0,671	0,528	0,505	0,539	0,605	0,542	0,694	0,702
RV	0,607	0,537	0,971	0,718	0,884	0,624	1036	0,768	0,694	1082	1135	0,830	0,916	0,508	0,575	0,501	0,768	0,521	0,913	0,925
ULL	0,387	0,488	0,536	1124	1389	0,971	1567	1219	1104	1611	1667	1299	0,540	0,553	0,402	0,607	0,176	0,542	0,328	0,344
LLL	0,612	0,606	0,994	0,815	0,968	0,726	1116	0,860	0,789	1144	1191	0,896	0,968	0,613	0,596	0,626	0,664	0,605	0,858	0,871
URL	0,559	0,718	0,339	1400	1666	1247	1847	1496	1377	1890	1946	1573	0,368	0,803	0,616	0,857	0,336	0,817	0,230	0,235
LRL	0,598	0,740	0,411	1415	1681	1262	1862	1511	1392	1905	1961	1589	0,445	0,821	0,642	0,874	0,408	0,831	0,308	0,311

Note: The distance is classified into three categories, green for distances less than 0.5, yellow for distances between 0.51 and 0.80, and orange for distances greater than 0.81.

Abbreviations: DAo, descending aorta; DR, distal rib; IAS, interatrial septum; IVS, interventricular septum; LA, left atrium; LLL, lower left lung; LRL, lower right lung; LV, left ventricle; LVW, left ventricular wall; MV, mitral valve; PM, papillary muscle; PR, proximal rib; RA, right atrium; RV, right ventricle; RVW, right ventricular wall; TV, tricuspid valve; ULL, upper left lung; URL, upper right lung.

TABLE 3 Mean embedment distances within structures and between structures in the axial cut fetal abdomen image for standard biometry.

Structure	PR	Column	DR	Skin	GW	LA	RA	UV	GC	Liver
PR	0,498	0,684	0,879	0,515	0,659	0,525	0,543	0,907	1509	1401
Column	0,639	0,350	1186	0,648	0,400	0,625	0,530	1273	1918	1801
DR	1010	1211	0,624	0,883	1349	0,906	0,993	0,634	0,805	0,721
Skin	0,740	0,788	0,941	0,720	0,823	0,723	0,728	0,974	1407	1305
GW	0,575	0,265	1312	0,676	0,170	0,638	0,495	1381	2026	1915
LA	0,441	0,613	0,710	0,395	0,655	0,385	0,408	0,764	1409	1295
RA	0,565	0,568	1005	0,563	0,598	0,537	0,497	1058	1576	1484
UV	0,909	1260	0,479	0,779	1375	0,813	0,932	0,454	0,685	0,578
GC	1514	1913	0,794	1377	2029	1416	1564	0,721	0,382	0,397
Liver	1400	1792	0,645	1256	1912	1295	1444	0,568	0,380	0,345

Note: The distance is classified into three categories, green for distances less than 0.5, yellow for distances between 0.51 and 0.80, and orange for distances greater than 0.81.
Abbreviations: CR, distal rib; GC, gastric chamber; GW, gastric wall; LA, left adrenal; PR, proximal rib; RA, right adrenal; UV, umbilical vein.

TABLE 4 Mean embedment distances within structures and between structures in the longitudinal section of the placenta.

Structure	AF	MP	LP	MPl	FPl	RPS
AF	0,347	0,715	1034	1529	1437	1411
MP	0,738	0,443	0,606	1343	1210	1144
LP	1054	0,588	0,469	0,996	0,862	0,797
MPl	1514	1300	0,967	0,354	0,408	0,451
FPl	1437	1172	0,815	0,453	0,416	0,428
RPS	1415	1118	0,760	0,484	0,426	0,417

Note: The distance is classified into three categories, green for distances less than 0.5, yellow for distances between 0.51 and 0.80, and orange for distances greater than 0.81.
Abbreviations: AF, amniotic fluid; FPl, fetal plate; LP, lateral placenta; MP, medial placenta; MPl, maternal plate; RPS, retroplacental space.

TABLE 5 Results of the application of Pearson's correlation coefficient test to the means of paired Euclidean distances of selected structures.

Image	Structure 1	Structure 2	*p*
Skull	PT	DT	0.8271
	0,41 887	0,42 897	
	ITM	CP	0.0000
	0,3678	0,87 394	
Thorax	MV	TV	0.7045
	0,14 932	0,1531	
	RVW	ULL	0.0000
	0,40 579	141 024	
Abdomen	LA	RA	0.4899
	0,38 482	0,4081	
	RA	Liver	0.0000
	0,49 724	148 423	
Placenta	MP	LP	0.0000
	0,44 284	0,60 556	
	MPl	FPl	0.7499
	0,41 605	0,40 792	

Note: A significant *p* result (<0.016) is observed between structures with presumed different biology and non-significant *p* in those recognized with similar histology in the different fetal and ovular ultrasound sections.
Abbreviations: CP, choroid plexus; DT, distal thalamus; FPl, fetal plate; ITM, interthalamic midline; LA, left adrenal; LP, lateral placenta; MP, middle placenta; MPl, maternal plate; MV, mitral valve; PT, proximal thalamus; RA, right adrenal; RVW, right ventricular wall; TV, tricuspid valve; ULL, upper left lung.

the application did not differentiate the texture of the segmented portion with statistical significance ($p = 0.827$), which allows us to think that it is a relevant application for texture discrimination, despite the acoustic shadow consistently found in this plane by the proximal fetal cap. On the other hand, in the images of the fetal thorax, the application showed statistically significant differences between the distance to the centroid of the descriptors of histologically different structures, of the 20 labeled for this cut, including the discrimination between structures with myocardial texture and lung texture. ($p = 0.000$). But it did not show significant or visual differences for similar structures, such as the mitral and tricuspid valve of the fetal heart ($p = 0.704$), showing how structures with a similar histological appearance are represented in this way by the application in terms of their texture. In the images of the fetal abdomen, the results were consistent when differentiating structures with different biological attributes in a statistically significant way, even to the point of discriminating the texture of the adrenal gland and liver ($p = 0.000$) and not differentiating structures that are histologically related such as the right and left adrenal ($p = 0.067$), structures whose identification in ultrasound can represent a challenge depending on the expertise of the examiner and the cut achieved, but which the application was able to recognize as similar regardless of their ultrasound appearance in terms of grayscale

or noise. Finally, in the placenta slices, in the six labeled structures, the ability to distinguish differences and texture similarities graphically and numerically was preserved, being striking how consistently and statistically significant ($p = 0.000$) managed to mark the differences between the middle and lateral segments of the placenta, plausible from the biological point of view due to the conformation and vascular distribution of this organ.

Until now, segmentation techniques in 2D fetal ultrasound images have been applied mainly for the automation of recognition of anatomical structures and standard fetal biometrics: gestational sacs or embryos by CRL,[16,17] biometry of the fetal head, abdomen and femur.[10] In fetal echocardiography its use has been for the calculation of measures that improve the diagnosis of heart disease through techniques that optimize the images, quantification and segmentation of the same.[18] In the fetal brain, segmentation techniques have been included in intelligent training algorithms to classify a brain as normal or abnormal in a 2D ultrasound image.[19] And finally, they have also been used to generate, in a semi-automated manner, the regions of interest of placentas in early pregnancies and extract information from the placental volume.[20]

As a strength of the study, we can determine that, within the known state of the art, it is the first study applying segmentation and texture characterization techniques to fetal ultrasound images that we are aware of to date, in an interactive framework that allows the specialist to adjust parameters and improve the segmentation, to successfully structure differentiation. As a weakness, we recognize that the segmentation technique used is still not an automatic procedure since, at the moment it is based on the distinction by the operator of the intensity level and similarity level thresholds, which constitutes a research work plan in the future that involves the knowledge acquired in this publication. Finally, the descriptors can be complemented by other characteristics that allow better quantifying the texture patterns in ultrasound images. The ultrasound exposure times during the study were not modified concerning standard practice since the acquisition process corresponds to the same protocol for routine obstetric imaging evaluation. The clinical relevance of the obtained results lies in the possibility of knowing the differences in texture of organs associated with maternal and fetal pathologies, which the human vision system cannot recognize and requires this type of processing to be evident. Furthermore, this type of study can be used to generate a knowledge base that can be integrated into subsequent stages of characterization and machine learning, to finally generate modifications in the ultrasound software that provide real-time assistance in recognition and segmentation of structures of interest at the fetal level.

In conclusion, the texture characterization of the labeled structures in the ultrasonographic images of the placenta, skull, thorax, and fetal abdomen by means of the numerical descriptors used through the application developed in the MATLAB mathematical processing software allows the discrimination of structures by level of showing similarity with the structures known biologically as similar and allowing the distinction of those different. These results represent the beginning for future works of tissue characterization in obstetric ultrasound that expand the information in the image and refine the accuracy of prenatal diagnoses.

ACKNOWLEDGMENTS

To the Quindío University's Engineering Program, to allow to use of the MATLAB software in the solidarity extension project modality.

CONFLICT OF INTEREST STATEMENT

The authors declare no conflict of interest.

DATA AVAILABILITY STATEMENT

The data that support the findings of this study are available from the corresponding author upon reasonable request.

ORCID

Saulo Molina-Giraldo https://orcid.org/0000-0001-6019-938X
Natalia Torres-Valencia https://orcid.org/0000-0001-9345-2847

REFERENCES

1. Burstein L. *Primary MATLAB® for Life Sciences*. Guide for Beginners. 2013.
2. Demirkaya O, Asyali MH, Sahoo PK. *Image Processing with MATLAB: Applications in Medicine and Biology*. CRC Press; 2008.
3. Rafael C, Gonzalez REW, Eddins SL. *Digital Image Processing Using*. Prentice-Hall, Inc.; 2003.
4. Qidwai U, Chen C-h. *Digital Image Processing: an Algorithmic Approach with MATLAB*. CRC press; 2009.
5. Dass R, Devi S. Image segmentation techniques 1. 2012.
6. Al-Amri SS, Kalyankar NV. Image segmentation by using threshold techniques. arXiv Preprint arXiv:10054020. 2010.
7. Kaur D, Kaur Y. Various image segmentation techniques: a review. *Int J Comput Sci Mob Comput*. 2014;3(5):809-814.
8. Norouzi A, Rahim MSM, Altameem A, et al. Medical image segmentation methods, algorithms, and applications. *IETE Tech Rev*. 2014;31(3): 199-213.
9. Reyes-Aldasoro CC. *Biomedical Image Analysis Recipes in MATLAB: for Life Scientists and Engineers*. John Wiley & Sons; 2015.
10. Rueda S, Fathima S, Knight CL, et al. Evaluation and comparison of current fetal ultrasound image segmentation methods for biometric measurements: a grand challenge. *IEEE Trans Med Imaging*. 2014; 33(4):797-813.
11. Van der Maaten L, Hinton G. Visualizing Data using t-SNE. *J Mach Learn Res*. 2008;9(86):2579-2605.
12. Lee L, Liew S. Breast ultrasound automated ROI segmentation with region growing. 4th International Conference on Software Engineering and Computer Systems (ICSECS). 2015 177–182.
13. ISUOG. ISUOG practice guidelines: ultrasound assessment of fetal biometry and growth. *Ultrasound Obstet Gynecol*. 2019;53(6): 715-723.
14. Buitrago Leal M, Beltran Avendaño M, Molina GS. Guias para la realización de ultrasonido obstétrico II y III trimestre. *Federación Colombiana de Asociaciones Ed perinatología - FECOPEN. Guias y suplementos*. 2014;1:13-22.
15. Anjna EA, Er RK. Review of image segmentation technique. *Int J Adv Res Comput Sci*. 2017;8(4):36-39.
16. Sobhaninia Z, Rafiei S, Emami A, et al. Fetal ultrasound image segmentation for measuring biometric parameters using multi-task deep learning. *Conf Proc IEEE Eng Med Biol Soc*. 2019;2019:6545-6548.

17. Sree SJ, Vasanthanayaki C. Ultrasound fetal image segmentation techniques: a review. *Curr Med Imaging Rev*. 2019;15(1):52-60.
18. Garcia-Canadilla P, Sanchez-Martinez S, Crispi F, Bijnens B. Machine learning in fetal cardiology: what to expect. *Fetal Diagn Ther*. 2020; 47(5):363-372.
19. Xie H, Wang N, He M, et al. Using deep learning algorithms to classify fetal brain ultrasound images as normal or abnormal. *Ultrasound Obstet Gynecol*. 2020;56:579-587.
20. Oguz I, Yushkevich N, Pouch A, et al. Minimally interactive placenta segmentation from three-dimensional ultrasound images. *J Med Imaging (Bellingham)*. 2020;7(1):014004.

How to cite this article: Molina-Giraldo S, Torres-Valencia N, Torres-Valencia C, Restrepo HF. Anatomical structure characterization of fetal ultrasound images using texture-based segmentation technique via an interactive MATLAB application. *J Clin Ultrasound*. 2023;1-12. doi:10.1002/jcu.23604